Thermal Response of Self-Organization in an Amphiphilic Triblock Polyelectrolyte and the Influence of the Globular Protein Lysozyme

Aristeidis Papagiannopoulos[1,*], Anastasia Meristoudi[1], Stergios Pispas[1,*] and Uwe Keiderling[2]

[1]Theoretical and Physical Chemistry Institute, National Hellenic Research Foundation, 11635 Athens, Greece

[2]Helmholtz Zentrum Berlin, D-14109 Berlin, Germany

* pispas@eie.gr

* apapagiannopoulos@eie.gr

Abstract

The associative, thermoresponsive and complexation properties of the triblock terpolymer PnBA-b-PNIPAM-b-PAA are explored in aqueous solutions. Using light scattering and small angle neutron scattering PnBA-b-PNIPAM-b-PAA is found to self-organize in aggregates of interconnected chains that are incorporated in larger clusters. Upon temperature increase the aggregates increase in molecular mass and shrink due to the enhancement of the hydrophobic interactions during the hydrophilic-to-hydrophobic transition of PNIPAM. In this state the well-defined aggregate interface gives rise to inter-aggregate spatial correlations. Remarkably the incorporation of lysozyme globules induces spatial correlations even at room temperature and controls the aggregate interconnections and mutual arrangement by tuning their surface charge and roughness. This system may be considered as a multicomponent, multifunctional super-structure with tunable morphology that combines the properties of synthetic and biological macromolecular components.

Keywords

thermoresponsive; block copolymers; proteins; complexation; small angle neutron scattering; aggregates

1. Introduction

Interaction of proteins with synthetic and biological polyelectrolytes is a subject of particular interest in biotechnological applications[1]. The nature of their complexation has been described by electrostatic and hydrophobic interactions. Additionally charge regulation[2] where a protein adjusts its charge to the local electrostatic environment and counterion release[3] where entropy drives the association of polyelectrolytes with proteins have been employed for the explanation of attraction of polyelectrolytes with proteins of net charge of the same sign. Detailed morphological description of the arrangement of globular proteins within spherical polyelectrolyte brushes of linear polyelectrolytes end-grafted on spherical nanoparticles has been established with small angle X-ray scattering[4]. In other works the aggregation state and internal arrangement of protein globules in polyelectrolyte/protein complexes has been revealed by small angle neutron scattering[5]. Recently we have used small angle neutron scattering to investigate self-assembled micelles from amphiphilic block polyelectrolytes as protein nanocarriers[6]. The incorporation of protein globules was detected on the measured form factors and it was also found to lead to organization of the polyelectrolyte micelles in a higher hierarchical level in a tunable manner.

Thermoresponsive character in synthetic macromolecules with interest in biomedical applications is often introduced by poly(N-isopropylacrylamide) (PNIPAM) blocks [7]. PNIPAM[8] has a lower critical solution temperature (LCST) at 32 °C which is between the room and the body temperature with obvious implications in drug delivery[9]. In copolymers based on N-isopropylacrylamide and chargeable groups

the thermal transition has been used to control the separation of the enzyme soybean peroxidase from solution[10]. The binding of lysozyme with butyl–modified thermoresponsive polymers poly(allylamine)s was influenced by both the increase in hydrophobicity and change in conformation above the LCST at a pH range where both protein and polymer were positively charged[11]. Encapsulation of bone morphogenetic proteins by elastin-like polymers was proved to relate to the polymer hydrophobic nature above its transition point[12]. In earlier studies thermoresponsive polymers with phase transitions at biologically relevant temperatures controlled hydrophobicity and bioadhesion at surfaces[13]. Grafted thermoresponsive polyelectrolytes have been used in thermoresponsive protein adsorption chromatography for protein purification[14] and thermoresponsive affinity chromatography[15]. Adsorption of fibrinogen on binary PAA/PNIPAM brushes was enhanced above the coil-to-globule transition when PNIPAM was in excess while it decreased when PAA was more than 50%[16].

Complexation of lysozyme with aggregates of the triblock terpolymer poly(ethylene oxide)-b-poly(N-isopropylacrylamide)-b-poly(acrylic acid) (PEO-b-PNIPAM-b-PAA) enhances hydrophobic interactions and inter-aggregate associations in PNIPAM-containing triblock polyelectrolytes while it makes thermoresponsive transitions totally irreversible[17]. In poly(n-butyl acrylate)-b-poly(N-isopropylacrylamide)-carboxylic acid (PnBA-b-PNIPAM-COOH) self-assembled core-shell micelles a length-scale and concentration dependent thermal transition was observed and was affected by interactions with lysozyme[18]. The charged carboxylic end-group stabilized the system during the hydrophilic-to-hydrophobic transition of PNIPAM while lysozyme globules accumulated near the micellar cores. In the case of poly(n-butyl acrylate)-b-poly(acrylic acid) (PnBA-b-PAA) the hydrated charged outer shell

of PAA was responsible for the interactions with the oppositely charged lysozyme and this led to intermicellar bridging associations [6].

In this article we investigate the self-assembling and thermoresponsive behavior of poly(n-butyl acrylate)-b-poly(N-isopropylacrylamide)-b-poly(acrylic acid) (PnBA-b-PNIPAM-b-PAA) and the effects upon addition of lysozyme in aqueous solutions. This triblock terpolymer is expected to have tunable hierarchical morphology at aggregate and inter-aggregate level and thermoresponsive behaviour that should be controlled by the incorporation of oppositely charged protein globules. We use light scattering methods to extract the size and the surface charge of the aggregates and complexes with lysozyme and to map their thermoresponsive transition. Small angle neutron scattering is performed to resolve the response of the internal organization of PnBA-b-PNIPAM-b-PAA aggregates in the presence and absence of lysozyme. This work illustrates the ability of multi-block stimuli-responsive copolymers to self-organize and respond at several length scales and the possibility to alter these properties by interactions with biological components.

2. Experimental

2.1 Materials

Synthesis and characterization of PnBA-b-PNIPAM-b-PAA

The synthesis of the PnBA-b-PNIPAM-b-PAA triblock terpolymer was performed using the reversible addition fragmentation chain transfer radical polymerization technique (RAFT)[19]. Polymerizations were run typically at c.a. 20%wt/v monomer concentrations. Firstly, the PnBA block was synthesized in one step polymerization of nBA monomer (0.5 g) using 2-dodecylsulfanylthiocarbonylsulfanyl-2-methylpropionic acid (0.25 mmol), as the RAFT CTA agent, in the presence of AIBN (as a 3×10^{-5} mol/mL solution in dioxane) as the polymerization initiator (moles AIBN

: moles CTA = 1:5), at 65^{o}C over 15 h in 1,4-dioxane. The resulting homopolymer was isolated and purified by precipitation into excess diethyl ether twice (90% yield, $M_{w,\ SEC}$ = 2.000, M_w/M_n = 1.09). Then, the PnBA-b-PNIPAM block copolymer was synthesized by using the PnBA block (0.45 g, 0.22 mmol) as the macro-RAFT agent and N-isopropyl acrylamide monomer (5g). The synthesis occurred at 65^{o}C for 15 h in the presence of AIBN (moles AIBN : moles macroCTA = 1:10), using 1,4-dioxane as the solvent. The desired block copolymer was precipitated twice into diethyl ether and was left to dry under vacuum prior to use (95% yield, $M_{w,\ SEC}$ = 21,800, M_w/M_n = 1.23). Finally, PnBA-b-PNIPAM-b-PAA triblock terpolymer was synthesized by the copolymerization of acrylic acid (AA, 6.2g) with the PnBA-b-PNIPAM block copolymer (5.1g). In this case PnBA-b-PNIPAM played the role of the macro-RAFT agent. The polymerization conditions were the same as those described for the synthesis of the PnBA-b-PNIPAM block copolymer, i.e. 65^{o}C for 15 h in the presence of AIBN, using 1,4-dioxane as the solvent. The resulting triblock terpolymer PnBA-b-PNIPAM-b-PAA, after precipitation in diethyl ether and drying under vaccum (95% yield), was characterized by SEC,^{1}H-NMR and FTIR and it was found to have the expected structure and chemical composition ($M_{w,SEC}$ = 45,200, M_w/M_n = 1.35, composition from ^{1}H-NMR: 4.5%wtPnBA, 43%wt PNIPAM, 52.5%wt PAA). The synthesis procedure and structure of PnBA-b-PNIPAM-b-PAA triblock terpolymer is presented in scheme 1. The degrees of polymerization of the blocks are N_{PnBA}=16, N_{PNIPAM}=170 and N_{PAA}=326. SEC, ^{1}H NMR and FTIR characterization data are provided in the Supplementary Material.

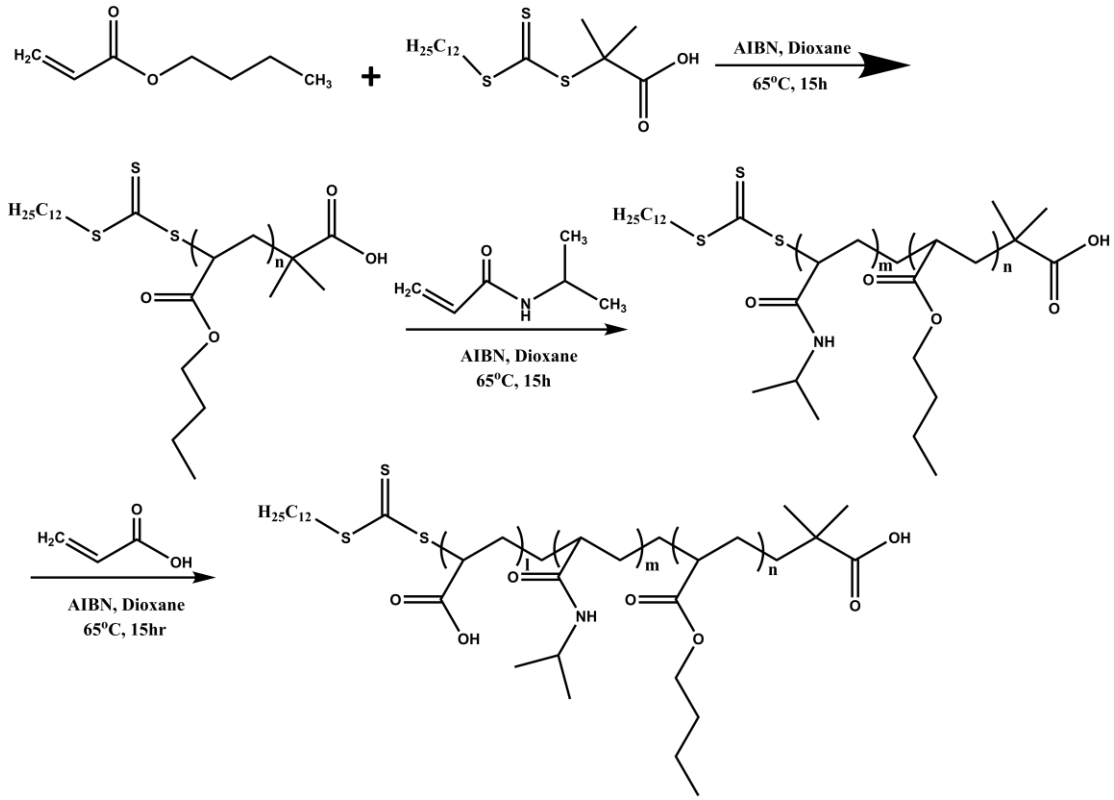

Scheme 1: Synthetic route for PnBA-b-PNIPAM-b-PAA triblock terpolymer.

Sample preparation

The triblock terpolymer is not readily dissolved in water and hence an alternative protocol was used. For a stock aqueous solution of 4 mg/ml polymer powder of 40 mg was dissolved in 1 ml tetrahydrofuran (THF, from Fluka, UV spectroscopy grade) which is a good solvent for all three blocks of the triblock, at 60°C for 5-6 hours. The THF solution was then added rapidly to 10 ml of H_2O (for light scattering) or D_2O (for small angle neutron scattering) under vigorous stirring. THF was removed by evaporation at 10 ºC in a rotor evaporator. NaCl was used to set the ionic strength at 0.01M. The pH was fixed at pH 7 by NaOH (in H_2O) and NaOD (in D_2O). For light scattering all sample solutions were filtered with 0.45μm PVDF membrane filters in order to remove any large aggregates or dust particles. The polymer concentration was 0.5 mg/ml so that multiple light scattering was negligible.

Hen egg white lysozyme (HEWL, M_w=14,300 g/mol) was purchased from Fluka and used without further purification. HEWL was dissolved at 1 mg/ml in H_2O or D_2O (pH7 and 0.01M NaCl). The lysozyme solutions were left overnight to equilibrate and for the isotopic exchange[20] to take place in D_2O. The target concentrations for the polymer and polymer/protein mixtures were produced from the parent solutions mixing the desired sample and D_2O or H_2O (pH 7 and 0.01M salt) volumes. At pH~7 lysozyme's net charge is about +7 while PAA have about 80% of their units (negatively) charged. Stable complexes were found at relatively low protein contents. The protein-to-polymer charge ratios [+]/[-] in solution were in the range 0.35-3.5% for light scattering and 0.3-1.2% for small angle neutron scattering.

2.2 Methods

Light Scattering

An ALV/CGS-3 compact goniometer system (ALVGmbH, Germany) in connection with a ALV-5000/EPP multi-tau digital correlator was used for the light scattering (LS) experiments. An He-Ne laser operating at the wavelength of 632.8 nm was the laser light source. In dynamic light scattering (DLS) we collected the intensity auto-correlation functions[21] at ~~90°~~ a broad angular range. The CONTIN algorithm was applied to obtain the distribution of characteristic relaxation times (τ).

$$R_h = \frac{k_B T}{6\pi\eta D} \qquad (1)$$

The distributions of hydrodynamic radii f(R_h) is calculated applying Stokes-Einstein relation (equation 1) and the equation $\tau^{-1}(q) = D \cdot q^2$ where the scattering wave vector is given by equation 2.

$$q = \frac{4\pi n_0}{\lambda} sin\frac{\theta}{2} \qquad (2)$$

where n_0 is the solvent's refractive index. η is the viscosity of the solvent, k_B is the Boltzmann constant and T is the absolute temperature. The average hydrodynamic radius is taken from the position of the maximum of the distribution function.

The sample temperature was set by a PolyScience controller while a 15 min wait-time was enough for the samples to equilibrate.

Electrophoretic light scattering

A Zetasizer Nano-ZS by Malvern Instruments Ltd was used for ζ-potential measurements. The calculation was performed by the Henry equation in the Smoluchowski approximation. The ζ-potential values reported are averages of 10–20 measurements taken at an angle of 173°.

Small angle neutron scattering

Small Angle Neutron Scattering (SANS) was performed on the instrument V4 (BERII Reactor at HZB). Three distinct sample-detector distance / wavelength configurations were used i.e. 16m/1.174nm, 4m/0.506nm and 1.35m/0.506nm. The range of the scattering wave vectors (q) covered was from 0.002 to 0.5 $Å^{-1}$. The scattered intensity I(q) is collected by a 2-D detector in the form of azimuthally isotropic patterns (normal for dilute solutions). The 2-D raw data were corrected for the scattering from the empty cell and the solvent and the electronic and background noise. The scattered intensities were calibrated to absolute units by a water (H_2O) standard The reduced 2-D data were azimuthally integrated to provide the 1-D I(q) profiles. The BerSANS software developed by U. Keiderling[22] was used for data reduction and integration. Resolution in scattering wave (Δq/q) vector[23] is taken into account by convoluting

the theoretically calculated I(q) with a Gaussian distribution as described elsewhere [18]. The standard deviation in wavelength of V4 ($\Delta\lambda/\lambda$=10%) is the dominant contribution and hence $\Delta q/q$=10%.

The data was fitted by minimizing the sum of the weighted square differences $\chi^2 = \sum_{i=1}^{N}\left(\frac{I^{conv}(q_i)-I^{exp}(q_i)}{\delta I^{exp}(q_i)}\right)^2$ between the N theoretical and experimental data points. The nonlinear least square optimization was performed by the Monte Carlo algorithm[24] in a simulated annealing process by custom made code in MATLAB.

The temperature of the samples was controlled with an accuracy of 0.1ºC and the samples were left to equilibrate for longer than 30 minutes at every set temperature.

3. Results and Discussion

3.1 Self-assembly of PnBA-b-PNIPAM-b-PAA in aqueous solutions

The DLS results show that there is one main relaxation mode in the solutions of PnBA-b-PNIPAM-b-PAA for all temperatures (figure 1a). The dependence of the characteristic relaxation rate (inverse characteristic time at the ~~single~~ main maximum of the distribution function) on q^2 is linear i.e. it shows diffusive behaviour (see Supplementary Material, figure S3a). The presence of a weaker maximum at about 20 and 13 nm at 21 and 25 °C respectively can be attributted to the presence of free aggregates (see discussion on SANS results). The contribution of smaller peaks at higher temperatures e.g. 32, 35 and 38 °C is negligible (representative intensity autocorrelation functions can be found in Supplementary Material, figure S3b). The hydrodynamic radius shows a rather broad transition as it systematically drops from 106 nm to 60 nm (figure 1a and 1b) in the temperature range 25 - 35 °C.

Scattered intensity at a fixed angle (usually 90°) is a sensitive probe of structural changes in solution and especially of critical transition temperatures[25-27]. Although scattered intensities depend both on molar mass and on scattering angle abrupt

changes in their magnitude are clear indications of transitions that affect self-assembly. Additionally in this study in the presence of lysozyme (section 3.2) the observed sizes are too large for a Guinier regime to be properly defined within the q-window of static light scattering. Hence we chose to present scattered intensity at a fixed angle for the sake of a uniform as well as a qualitative way to highlight the thermal transitions. The scattered light intensity at 90° increases significantly (~10 times) between 32 and 42 °C (figure 1c). This enhancement is possibly related to an increase in the apparent molar mass (as it will be quantitatively proved by SANS in the following) that accompanies a reduction in the gyration radius. Hence the hydrophilic-to-hydrophobic transition of PNIPAM leads to an increase in the apparent molecular mass due to interchain associations and a shrinkage of the overall aggregate size. Obviously the initially formed clusters interassociate and possibly the free small aggregates are incorporated to the larger clusters. This is in contrast to our previous work on solution behavior of PEO-b-PNIPAM-b-PAA where the thermally-triggered associations caused an increase in the overall size, although in an intermediate kinetic regime shrinkage was observed[17]. Probably the presence of a hydrophobic block (PnBA) instead of a hydrophilic one (PEO) favors the formation of collapsed aggregates rather than loose ones.

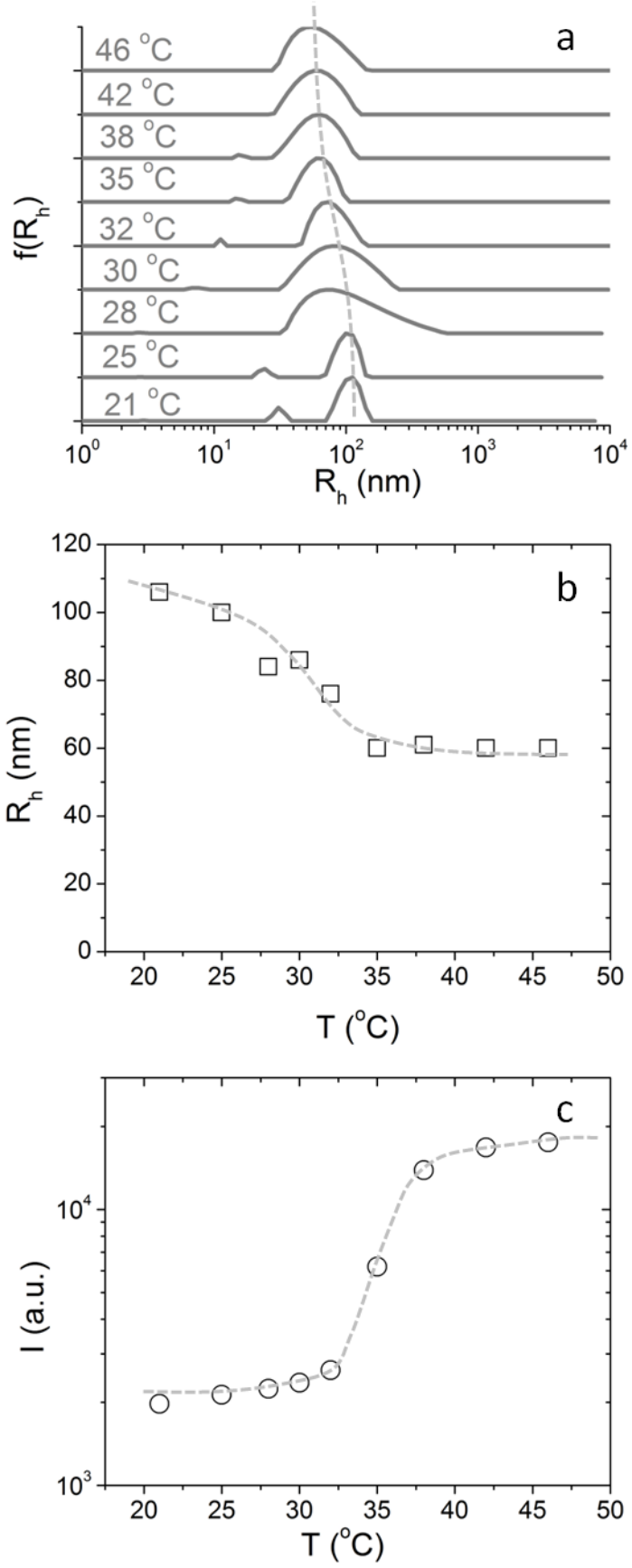
a
46 °C
42 °C
38 °C
35 °C
32 °C
30 °C
28 °C
25 °C
21 °C
f(R_h)
10^0
10^1
10^2
10^3
10^4
R_h (nm)
b
120
100
80
60
40
20
0
R_h (nm)
20
25
30
35
40
45
50
T (°C)
c
10^4
10^3
I (a.u.)
20
25
30
35
40
45
50
T (°C)

Figure 1: (a) Distribution of hydrodynamic radii (at θ=90°), (b) hydrodynamic radius (at θ=90°) and (c) scattered intensity (at θ=90°) of PnBA-b-PNIPAM-b-PAA in 0.5 mg/ml (0.01 M NaCl / pH 7) for different solution temperatures. Dashed lines are guides to the eye.

The SANS measurements were performed below and above the thermal transition temperature defined by LS i.e. at 25 and 50° C. At low temperature the scattered intensity was adequate for good statistics at a reasonable collection time only for the highest concentration (4.0 mg/ml). For the lower concentrations only the intermediate and high q data are presented (figure 2a). At high temperature the scattered intensity was significantly increased and allowed the collection at all camera lengths for all concentrations (figure 2b). The absence of any characteristic oscillation or weak bump in the SANS profiles (figure 2) indicates that the association of PnBA-b-PNIPAM-b-PAA does not lead to a well-separated core-shell morphology. Hydrophobic interactions between PNIPAM segments even below the LCST[28], between PAA segments since it is an intrinsically hydrophobic polyelectrolyte and consequently between PNIPAM and PAA segments are possible. The presence of PnBA hydrophobic blocks may surely enhance the hydrophobically driven associations. The degree of polymerization in PnBA (N_{PnBA}=16) is much lower than the one of PNIPAM (N_{PNIPAM}=170) or PAA (N_{PAA}=326). This way it could be preferable for a random network of hydrophobic contacts to be created instead of a core-shell micellar structure. In our previous work on the diblock copolymer PnBA-b-PNIPAM-COOH (N_{PnBA}=24 and N_{PNIPAM}=65) which was end-functionalized with one carboxylic group we have found a core-shell morphology, but still both core and shell contained mixed PnBA and PNIPAM blocks[18]. On the other hand for PnBA-b-PAA (N_{PnBA}=94 and

N_{PAA}=170) we found a clearly separated hydrophobic core (PnBA) / hydrophilic corona (PAA) morphology[6]. Maybe except from the length of the hydrophobic block also the presence of PNIPAM is responsible for the mixing of hydrophobic and hydrophilic blocks inside the aggregates.

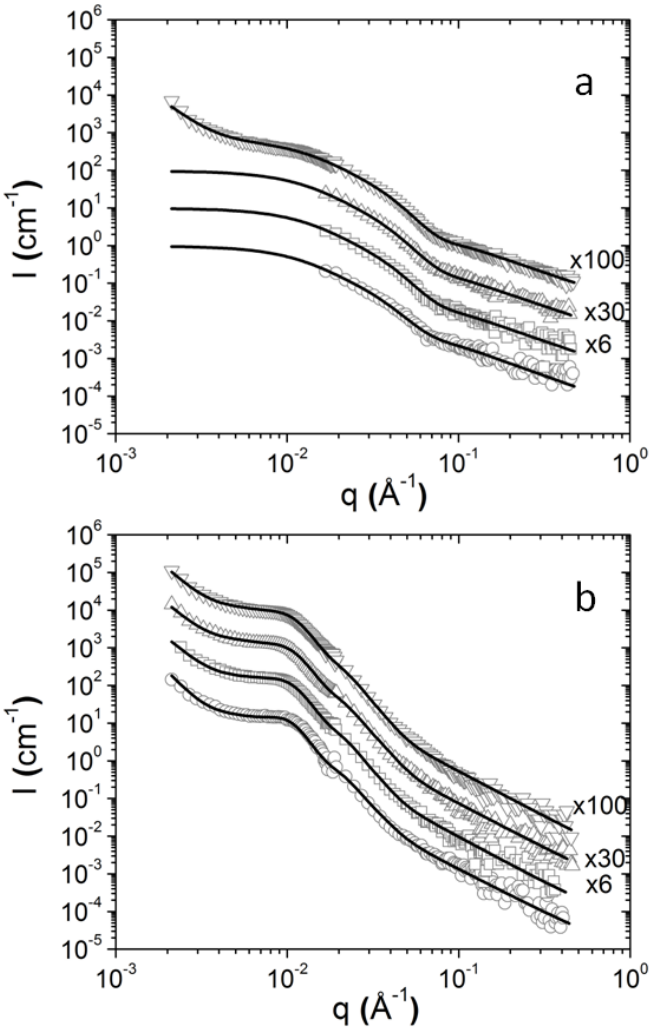

Figure 2: SANS profiles from PnBA-b-PNIPAM-b-PAA (0.01 M NaCl / pH 7) at 0.5 (○), 1.0 (□), 2.0 (△) and 4.0 (▽) mg/ml for (a) 25 and (b) 50 °C. Lines are fits to the experimental data.

As no characteristic oscillation or weak bumps were found in SANS profiles a three-level hierarchical model (equation 3) was used to fit the data. The unified

Guinier/power-law model was chosen to model the SANS data since it can extract the characteristic length scales and power-law trends with a minimal number of fitting parameters in aggregates with soft and polydisperse morphology. In the case of low temperatures (except from 4.0 mg/ml concentration) only the two terms that correspond to intermediate and high q are used.

$$I(q) = I_{fr}(q) + I_{agg}(q) \cdot S_{agg}(q) + I_{int}(q) \qquad (3)$$

At low q the power-law I_{fr} corresponds to fractal-type scattering caused by high-size clusters (equation 4). Equation 4 is modified[29] by a multiplying cut-off factor $\exp(-1/3 \cdot \mathrm{q}^2 \mathrm{R}_{\mathrm{cut}}^2)$. $\mathrm{R}_{\mathrm{cut}}$ is in the order of the radius of gyration (R_{g}) of the next smaller hierarchical level i.e. the one described by $I_{agg}(q)$.

$$I_{fr}(q) = \frac{B_{fr}}{q^{d_{fr}}} \qquad (4)$$

At intermediate q a unified Guinier/power-law Beaucage[30, 31] model $I_{agg}(q)$ represents the main scattering objects in solution which will be refered to as "aggregates" (equation 5). The prefactor of the power-law[30] is given by $B_{agg} = \frac{G_{agg} \cdot d_{agg}}{R_g^{d_{agg}}} \cdot \left[\frac{6{d_{agg}}^2}{(2+d_{agg})(2+2d_{agg})}\right]^{d_{agg}/2} \Gamma\left(\frac{d_{agg}}{2}\right)$. At low tepmperature and in the absence of lysozyme the structure factor contribution is not needed and hence $S_{agg}(q) = 1$.

$$I_{agg}(q) = G_{agg} \cdot exp\left(-\frac{q^2 R_g^2}{3}\right) + \frac{B_{agg}}{q^{d_{agg}}}\left[erf\left(\frac{qR_g}{\sqrt{6}}\right)\right]^{3d_{agg}} \qquad (5)$$

At high q a power-law (equation 6) is needed to fit the data and it comes from correlations within the formed aggregates. The characteristic length ξ_{int} is about 3.6 nm at 25 °C and about 8.5 nm at 50 °C.

$$I_{int}(q) = \frac{B_{int}}{q^{d_{int}}}\left[erf\left(\frac{q\xi_{int}}{\sqrt{6}}\right)\right]^{3d_{int}} \qquad (6)$$

At high temperature (figure 2b) the scattered intensity is modulated by a weak structure factor feature at about 0.01 Å^{-1}. The structure factor is given by equation 7 and represents structural correlations of colloidal particles[32] occurring at an average radial distance R_{cor}. The scattering amplitude is the one of a sphere given by $A(q) = 3 \cdot \frac{\sin(qR_{cor}) - qR_{cor}\cos(qR_{cor})}{(qR_{cor})^3}$. The packing factor k describes the degree of correlation and it is k<4 for weakly correlated systems. This factor is related to the number of nearest neighbors as for example in the case of hard spheres it is about 8 times their volume fraction φ. In figure 3, examples of the contribution of the three hierarchical levels and the modulation due to the structure factor are presented.

$$S_{agg}(q) = \frac{1}{1 + k \cdot A(q)} \qquad (7)$$

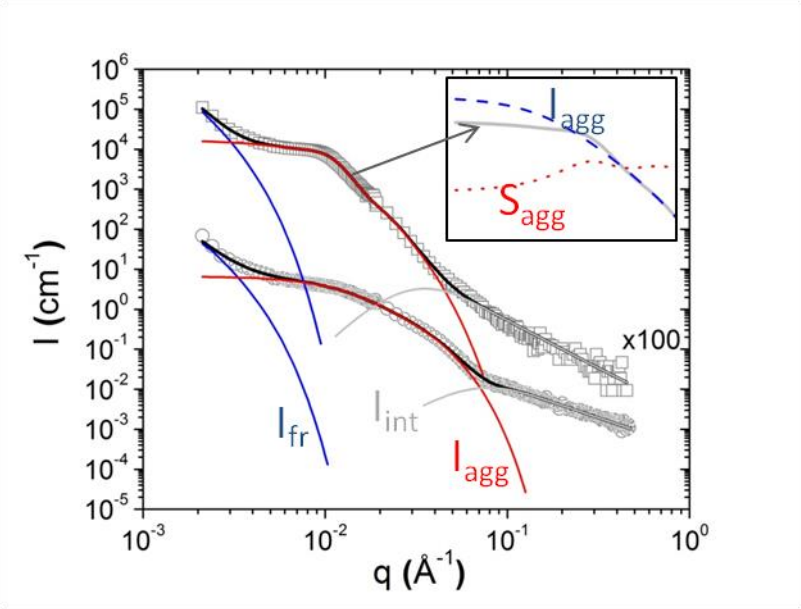

Figure 3: Contribution of separate contributions to the fitted SANS profiles from PnBA-b-PNIPAM-b-PAA (0.01 M NaCl / pH 7) at 4.0 mg/ml for 25 (○) and 50 (□) °C. Inset presents the structure factor modulation to I_{agg}.

Figure 4 presents the extracted parameters from the SANS experiments. The scattered intensities at 0.0022, 0.02 and 0.2 $Å^{-1}$ are chosen so as to compare the separate contributions of the different hierarchical levels (figure 4a). The intensity corresponding to a specific structural level is proportional to concentration either at low or high temperature showing that the morphology of the assemblies is concentration independent. Although the experimental information on the highest hierarchical level for the concentrations 0.5, 1.0 and 2.0 mg/ml is absent it can be safely assumed that the morphology at this level is also concentration independent. The independence of morphology on concentration is supported qualitatively by the unaltered shape of the SANS profiles and quantitatively by the extracted sizes (figure 4b) and characteristic exponents (figure 4c) that have constant values within experimental error.

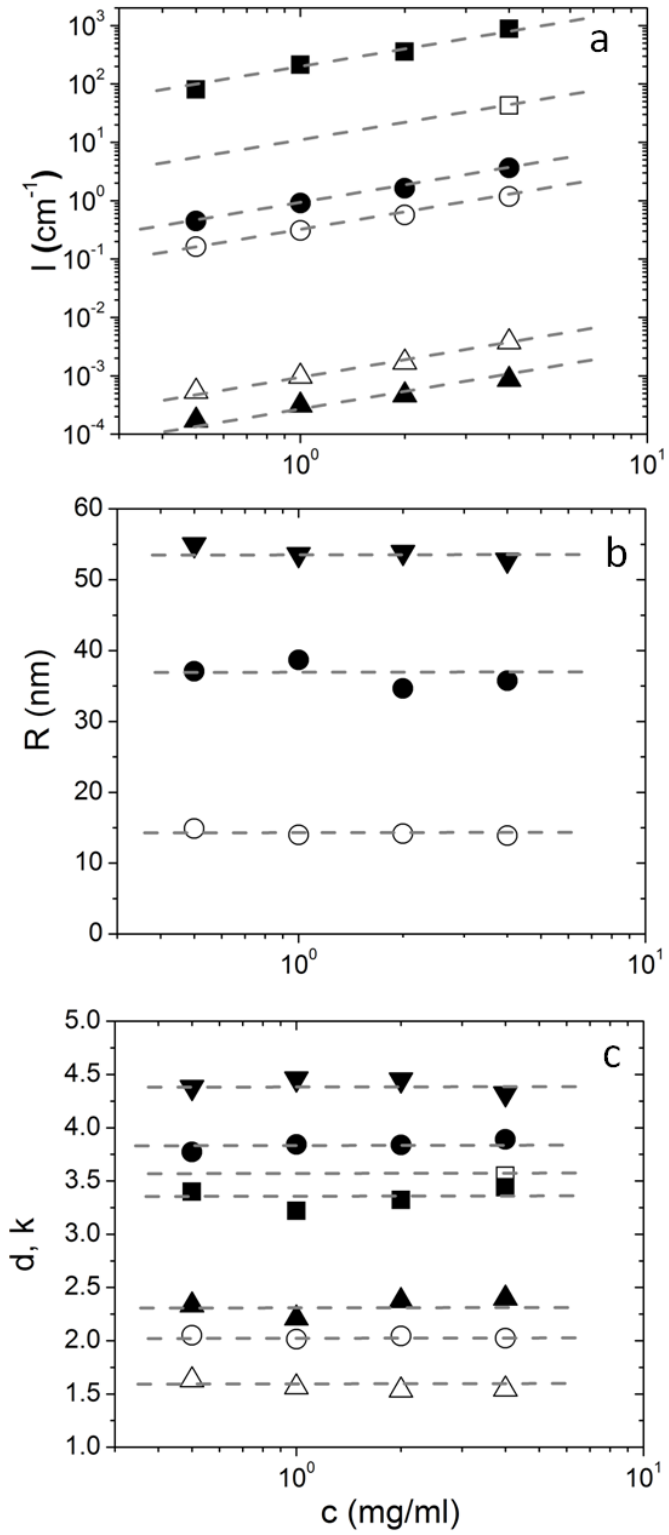

Figure 4: Parameters extracted from SANS in PnBA-b-PNIPAM-b-PAA (0.01 M NaCl / pH 7). (a) SANS intensity at 0.0022 (□), 0.02 (○) and 0.2 (△) Å^{-1}. (b) Radius

of gyration (R_g) of the aggregates (○) and radial distance (R_{cor}) of correlations (▽). (c) Characteristic exponents d_{int} (△), d_{agg} (○) and d_f (□) and degree of correlation k (▽). Open and closed symbols represent 25 °C and 50 °C respectively. Dashed lines are guides to the eye.

The scaling exponent d_{int} is 1.6 at room temperature and 2.4 at high temperature i.e. the morphology at small length scales changes from a sparse mass fractal to a dense mass fractal (figure 4c). The exponent 1.6 could be related to an average self-avoiding chain conformation of PAA and PNIPAM blocks within the aggregates. At higher temperatures PNIPAM is in its globular state while PAA has an increased number of hydrophobic contacts with neighboring chains which is compatible with d_{int}=2.4. This change in aggregate internal morphology causes a suppression to the related scattered intensity I(0.2 $Å^{-1}$). The exponents d_{agg} for the intermediate aggregates increase from 2 to 3.8. This clear transition from a mass fractal to a surface fractal with well-defined interface[33] is connected to the signature of hard-sphere interactions between the aggregates at 50 ºC. The scaling exponents d_f of the large clusters are in the range of rough surface fractals and are unaffected by temperature. In a recent study of PNIPAM-b-PEG-b-PNIPAM a hierarchical structure has also been revealed by SANS[34]. The distribution of the hydrophilic blocks was proved to be uniform within the aggregates while the thermoresponsive transition was found broad (as in our case) a fact that was attributed to the presence of PEG.

The characteristic R_g of the aggregates at 25 °C is ~15 nm (figure 4b) which is much lower than the value observed by DLS (~100 nm). This means that LS is sensitive to the presence of higher clusters of aggregates as it probes a lower q range ($7 \cdot 10^{-4}$-$3 \cdot 10^{-3}$ $Å^{-1}$). These clusters give rise to the fractal scattering $I_{fr}(q)$ at low q in SANS. The

aggregates increase in size at 50 °C with $R_g \approx 37$ nm. In this case the size is comparable to the one in DLS (ca. 60 nm). The characteristic correlation radius $R_{cor} \approx 53$ nm is even nearer the DLS values. Hence at high temperatures the aggregates observed in SANS correspond to the dominating entities in DLS.

The scattered intensity coming from the aggregates increases with temperature (figure 4a) which means that more PnBA-b-PNIPAM-b-PAA chains are accumulated within aggregates above the LCST which is in line with the trend in SLS intensity. From the extrapolated intensity from aggregates $I_{agg}(0) = G_{agg}$ and the molecular characteristics of the blocks (neutron scattering length density, molecular weight and mass density) the number of triblock chains within the aggregates can be extracted[35] (see Supplementary Material for details). At 25 °C there are about 16 chains in average within an aggregate while at 50 °C this number is 2500.

In SANS (figure 4a) the scattering from higher clusters is enhanced at high temperatures although this effect is not observed in DLS (since the aggregates are dominating DLS at high temperatures) pointing to the sensitivity of the system to the solvent type (D_2O for SANS / H_2O for LS). We have observed the isotope effect also in the case of PnBA-b-PAA where higher aggregation numbers[6] were observed in D_2O (SANS) in comparison to H_2O (LS). The hierarchical morphology of the system is illustrated in scheme 2. The coil-to-globule transition of PNIPAM leads to denser aggregates with better defined interface. As it will be discussed in the next section an increase in the surface charge during the transition shows that PAA segments are forced to the outer periphery of the aggregates and hence enhance the repulsive interactions. This is a stabilizing mechanism against the hydrophobicity of the system which increases. A similar mechanism has been illustrated recently[18] with PnBA-b-

NIPAM-COOH where a single charged unit at the free end of PNIPAM stabilizes the micelles.

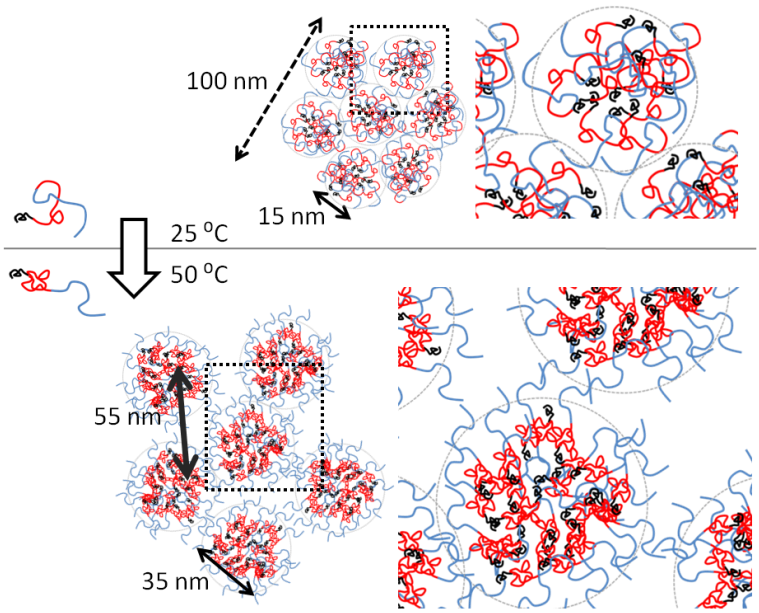

Scheme 2: Illustration of the PnB-b-PNIPAM-b-PAA organization in aqueous solution based on DLS and SANS. PnBA, PNIPAM and PAA blocks are depicted by black, red and blue respectively. The rectangular regions (marked by dashed line) are shown magnified in the right. The coil-to-globule transition of PNIPAM within a single PnB-b-PNIPAM-b-PAA chain is also depicted.

3.2 Interactions of PnBA-b-PNIPAM-b-PAA with lysozyme

The LS results (figure 5) show that lysozyme globules cause associations between the PnBA-b-PNIPAM-b-PAA aggregates. This is related to electrostatic interactions (lysozyme has a positive while PAA a negative charge at pH 7) and hydrophobic effects since lysozyme contains hydrophobic domains on its surface[36]. The attachment of positive lysozyme globules to the aggregates reduces the net charge of

the complexes and reduces their mutual repulsions. This leads to a significant increase in size (figure 5a) and scattered intensity (figure 5b).

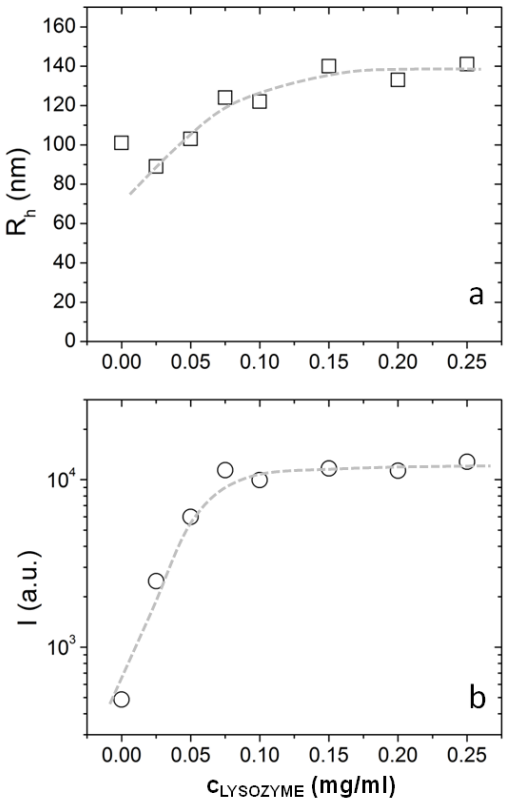

Figure 5: (a) Hydrodynamic radius and (b) scattered intensity of PnBA-b-PNIPAM-b-PAA in 0.5 mg/ml (0.01 M NaCl / pH 7) as a function of concentration of added lysozyme at 25 °C at scattering angle 90°. Dashed lines are guides to the eye.

The effect of temperature on the hydrodynamic radius of the complexes in the presence of lysozyme is qualitatively different than in its absence (figure 6a). Size distributions from complexes can be found in Supplementary Material (figure S4). Instead of a decrease, an increase in size (R_h up to ~5000 nm) takes place that shows that the temperature rise leads to associations of aggregates without a collapse in the large-scale morphology (loose clustering). The diffusive behavior of the characteristic relaxation mode in DLS is presented in Supplementary Material (figure S5). The

association of aggregates is confirmed by the behavior of the SLS intensity (figure 6b). The ζ-potential data (figure 6c) are reminiscent of the complexes of core-shell PnBA-b-PNIPAM-COOH with lysozyme[18]. Increasing temperature well above the LCST of the system increases the surface charge of the aggregates. Apparently the charged hydrophilic PAA units are pushed away from the increasingly hydrophobic interior. Lysozyme is able to induce charge reversal at high globule concentrations only at low temperature.

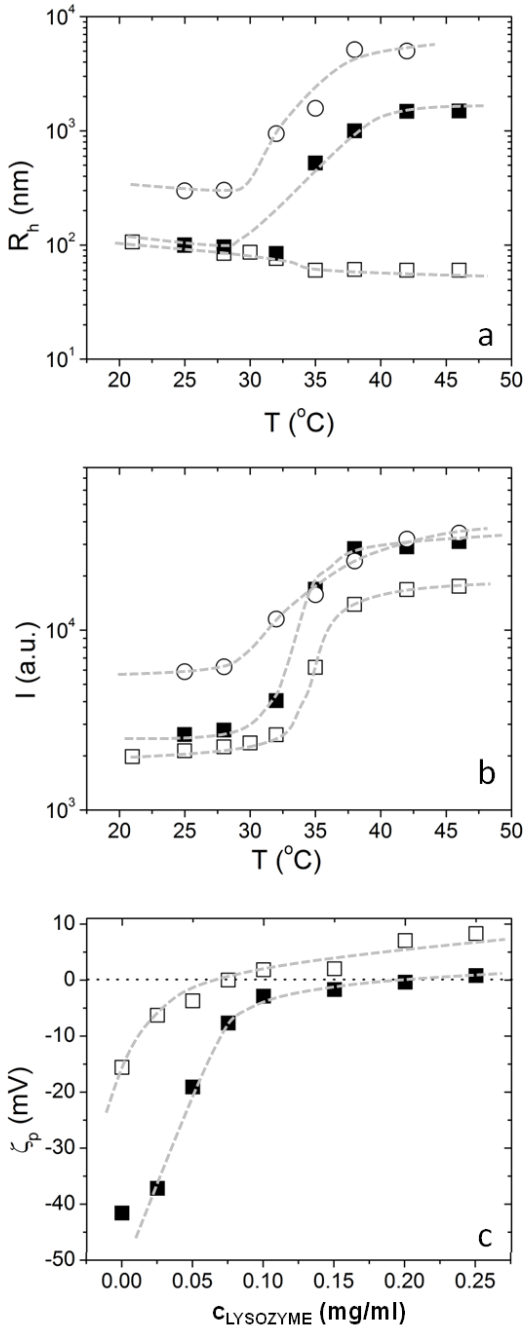

Figure 6: (a) Hydrodynamic radius and (b) scattered light intensity of PnBA-b-PNIPAM-b-PAA/lysozyme complexes with PnBA-b-PNIPAM-b-PAA 0.5 mg/ml and 0 mg/ml (□), 0.025 mg/ml (■) and 0.25 mg/ml (○) lysozyme (0.01 M NaCl / pH 7) as a function of temperature. (c) ζ-potential of complexes as a function of lysozyme concentration for 26 °C (□) and 42 °C (■).

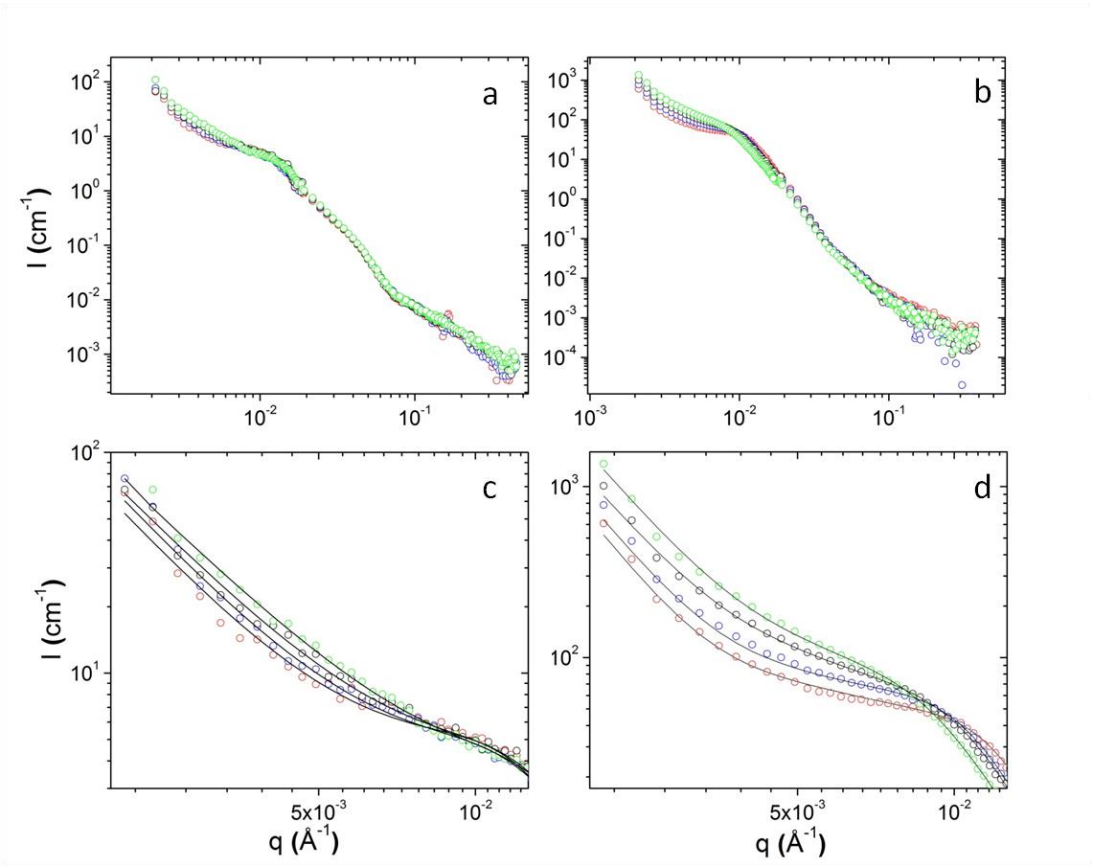

Figure 7: SANS profiles from PnBA-b-PNIPAM-b-PAA 2.4 mg/ml (0.01 M NaCl / pH 7) at 25 °C (a,c) and 50 °C (b,d) for 0.1 (red), 0.2 (blue), 0.3 (black) and 0.4 (green) mg/ml added lysozyme. The low q region has been magnified in c and d. Lines in c and d are fits to the experimental data.

The hydrodynamic radius of lysozyme is about 2 nm so that during interaction with PnBA-b-PNIPAM-b-PAA it can be thought of as a small spherical object entering a large polymeric aggregate[18]. In SANS (figure 7) it is clear that complexation of lysozyme enhances the low q scattering. This shows that lysozyme globules are attached to the outer regions of the intermediate aggregates without affecting their internal morphology. The last observation is in agreement with the loose clustering suggested by LS. In PnBA-b-PAA lysozyme appeared to bind to the outer parts of the hydrated micellar PAA corona tuning intermicellar clustering [6]. In PnBA-b-

PNIPAM-COOH complexation drove lysozyme near the micellar core and did not cause significant alterations on the intermicellar aggregation[18]. Lysozyme contains hydrophobic domains and charged patches. In the first case it interacted mainly via elactrostatic interactions with PAA (as it was also confirmed by measurements at different ionic strengths) while in the second case the hydrophobic interactions with PNIPAM and PnBA dominated (COOH is a single charged unit). Hence in PnBA-b-PNIPAM-b-PAA the outer charged blocks define the interactions with lysozyme.

The SANS data are fitted by equation 3 as it was done in the absence of lysozyme. In figures 7c and 7d the quality of the fits is illustrated in magnification. The systematic effect of protein complexation is stronger at high temperature where the charged units are pushed to the exterior of the aggregates. The extracted SANS parameters (figure 8) that are affected by lysozyme are consequently the ones related to low q or in other words to large and intermediate length scales. This can be also shown by comparing the SANS profiles without and with added protein (figure S6). The scattered intensity from clusters is systematically enhanced by the addition of protein globules. The temperature response of the scattered intensities is similar to the one in the absence of lysozyme.

It is very interesting that in the presence of lysozyme there are correlations between aggregates even at low temperature as the $S_{agg}(q)$ term of equation 7 is needed to model the data. In our previous work on PnBA-b-PNIPAM-COOH complexation with lysozyme hard-sphere correlations were observed only at high temperatures but were facilitated by the presence of lysozyme[18]. Here the incorporation of lysozyme at the outer periphery of the polymeric aggregates creates a denser interface (less rough) that induces hard-sphere interactions and causes measurable correlations even at low temperatures (figures 7 and 8c). Indeed the characteristic exponent d_{agg} is 2.7 at 25 ºC

(d_{agg} ≈2 in the absence of lysozyme) and 3.7 at 50 ºC (d_{agg} ≈ 3.8 in the absence of lysozyme). The packing factor k is independent of lysozyme concentration (k≈2.3) at low temperature while at high temperature drops systematically from 3.6 to 2 (figure 8c). This is followed by a strong increase in the correlation distance R_{cor} at high temperature while it is constant at low temperature (figure 8b) pointing to more effective repulsive hard sphere potential as the aggregates interface becomes occupied by more protein globules. While the increase in R_{cor} is obvious in the SANS profiles as a shift of the characteristic feature at the region of 0.01 $Å^{-1}$ to lower q the decrease in k could be artificially caused by the enhanced scattering of clusters that effectively smear the scattering profile at this q region and not by an actual decrease in the number of nearest neighbors.

At high q the power law is defined by a d_{int} about 1.4 at 25 °C and about 2.6 at 50 °C which are independent of lysozyme content and comparable to the values found in the absence of lysozyme (figure 4c). This shows that lysozyme globules do not disturb small length scale correlations significantly. The characteristic length ξ_{int} is about 4.2 nm at 25 °C and about 7.9 nm at 50 °C and are similar to the ones in the absence of protein.

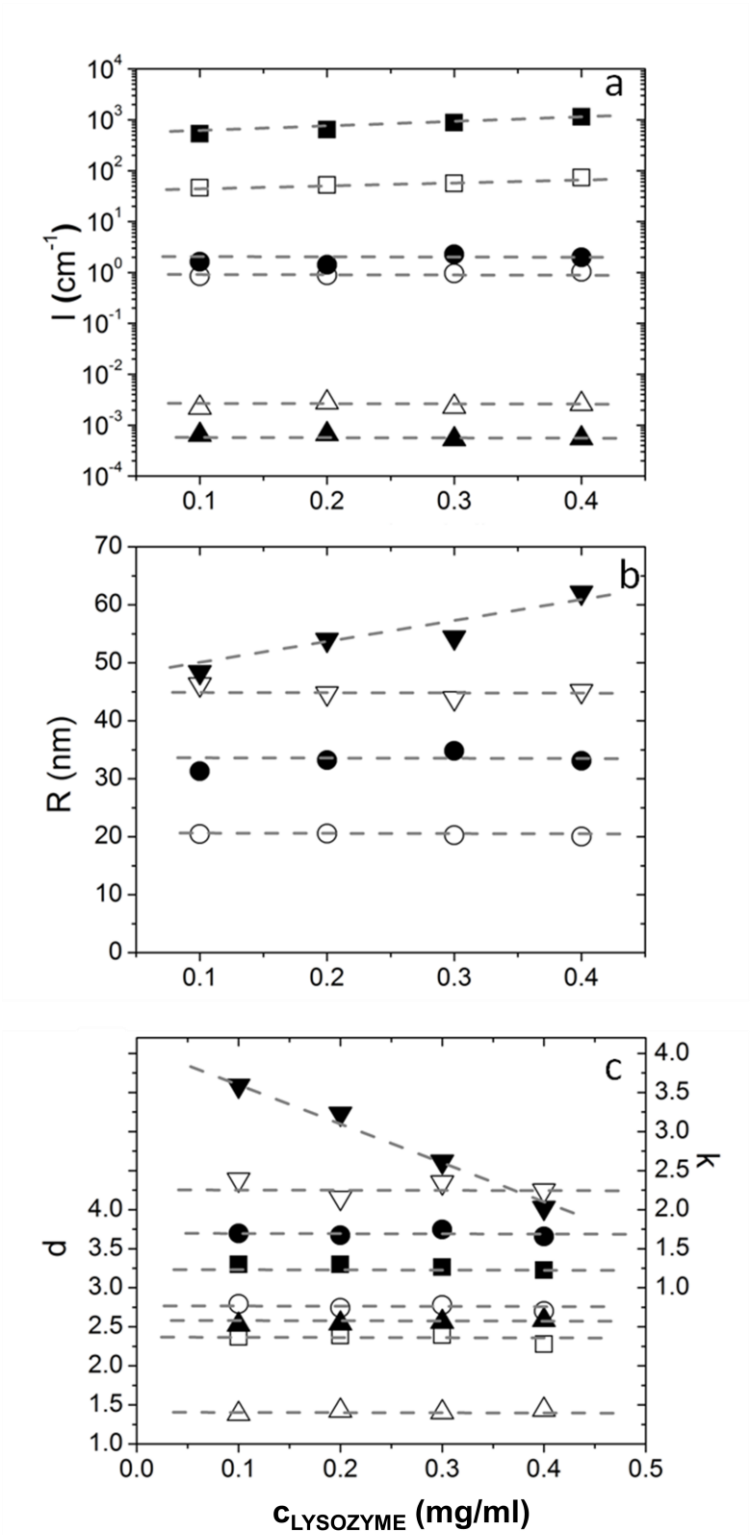

Figure 8: Parameters extracted from SANS in PnBA-b-PNIPAM-b-PAA/lysozyme complexes (0.01 M NaCl / pH 7) as a function of lysozyme concentration. (a) SANS intensity at 0.0022 (□), 0.02 (○) and 0.2 (△) Å^{-1}. (b) Radius of gyration (R_g) of the

aggregates (○) and radial distance (R_{cor}) of correlations (▽).(c) Characteristic exponents d_{int} (△), d_{agg} (○), d_f (□) and degree of correlation k (▽). Open and closed symbols represent 25 °C and 50 °C respectively. Dashed lines are guides to the eye.

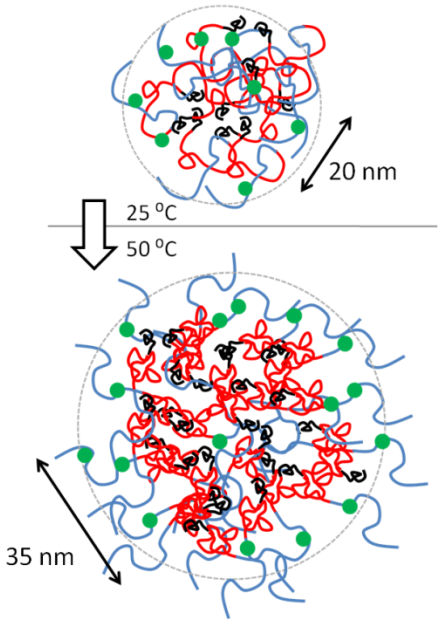

Scheme 3: Illustration of the aggregates morphology in PnB-b-PNIPAM-b-PAA/complexes in aqueous solution based on ELS and SANS. PnBA, PNIPAM and PAA blocks are depicted by black, red and blue respectively. Lysozyme globules are represented by green discs.

An illustration of the aggregates morphology in the presence of lysozyme is provided in scheme 3. Addition of protein at room temperature enhances the hydrophobic character of the aggregates and reduces the roughness of their interface. At high temperature their interface is better defined and contains mostly PAA segments and protein globules.

4. Conclusions

The self-assembly of the triblock terpolymer PnBA-b-PNIPAM-b-PAA was studied in aqueous solutions with light scattering and small angle neutron scattering methods. The morphology of the multi-chain aggregates transformed from low molecular weight soft particles to dense objects of well-defined interface with hard-sphere-type interactions during the PNIPAM coil-to-globule transition. Interaction with lysozyme enhanced the inter-aggregate associations and caused hard-sphere correlations at room temperature. Especially at high temperature lysozyme solution content can readily define the degree of aggregate clustering and the effective repulsive inter-aggregate interaction potential. These findings combine properties found in studies of PnBA-b-PAA and PnBA-b-PNIPAM-COOH block copolymers. In particular they show that the presence of a polymeric charged block (PAA) renders the interaction with lysozyme mainly electrostatic contrary to the case of a single COOH end-group where the interaction is mainly hydrophobic and controlled by PNIPAM and PnBA. This effect also defines the positioning of lysozyme globules within the aggregates and hence the inter-aggregate interactions. The studied system offers a template for creation of multi-level hierarchical hybrid multicomponent, multifunctional structures that can self-assemble in a tunable manner by controlling the temperature and the concentration of the biological component that may be potentially useful in biomedical applications, including protein drug delivery and enzyme based biotechnology.

5. Acknowledgements

The authors acknowledge financial support by the NANOMACRO 1129 project which is implemented in the framework of the Operational Program “Education and Life-long Learning” of the National Strategic Reference Program-NSRF (Action

“ARISTEIA I”) and it is co-funded by the European Union (European Social Fund-ESF).

This research project has been supported by the European Commission under the 7th Framework Programme through the 'Research Infrastructure' action of the 'Capacities' Programme, NMI3-II Grant number 283883.

6. References

[1] A.B. Kayitmazer, D. Seeman, B.B. Minsky, P.L. Dubin, Y. Xu, Protein-polyelectrolyte interactions, Soft Matter 9(9) (2013) 2553-2583.

[2] W.M. de Vos, P.M. Biesheuvel, A. de Keizer, J.M. Kleijn, M.A. Cohen Stuart, Adsorption of the Protein Bovine Serum Albumin in a Planar Poly(acrylic acid) Brush Layer As Measured by Optical Reflectometry, Langmuir 24(13) (2008) 6575-6584.

[3] A.L. Becker, K. Henzler, N. Welsch, M. Ballauff, O. Borisov, Proteins and polyelectrolytes: A charged relationship, Curr Opin Colloid Int Sci 17 (2012) 90-96.

[4] S. Rosenfeldt, A. Wittemann, M. Ballauff, E. Breininger, J. Bolze, N. Dingenouts, Interaction of proteins with spherical polyelectrolyte brushes in solution as studied by small-angle x-ray scattering, Phys. Rev. E 70 (2004).

[5] F. Cousin, J. Gummel, D. Ung, F. Boué, Polyelectrolyte−Protein Complexes: Structure and Conformation of Each Specie Revealed by SANS, Langmuir 21(21) (2005) 9675-9688.

[6] A. Papagiannopoulos, A. Meristoudi, S. Pispas, A. Radulescu, Micelles from HOOC-PnBA-b-PAA-C12H15 Diblock Amphiphilic Polyelectrolytes as Protein Nanocarriers, Biomacromolecules 17(11) (2016) 3816–3827.

[7] M.A. Ward, T.K. Georgiou, Thermoresponsive Polymers for Biomedical Applications, Polymers 3(3) (2011) 1215.

[8] C. Wu, X. Wang, Globule-to-Coil Transition of a Single Homopolymer Chain in Solution, Physical Review Letters 80(18) (1998) 4092-4094.

[9] D. Schmaljohann, Thermo- and pH-responsive polymers in drug delivery, Advanced Drug Delivery Reviews 58(15) (2006) 1655-1670.

[10] T.V. Burova, N.V. Grinberg, A.S. Dubovik, G. Zhang, V.Y. Grinberg, Interpolyelectrolyte complexes of soybean peroxidase with thermoresponsive copolymers, Polymer Science Series A 54(7) (2012) 573-584.

[11] J.-j. Liu, Y.-f. Yan, P. Yao, Binding of thermo-sensitive and pH-sensitive butylated poly(allylamine)s with lysozyme, Chinese Journal of Polymer Science 29(4) (2011) 397-406.

[12] P.C. Bessa, R. Machado, S. Nürnberger, D. Dopler, A. Banerjee, A.M. Cunha, J.C. Rodríguez-Cabello, H. Redl, M. van Griensven, R.L. Reis, M. Casal, Thermoresponsive self-assembled elastin-based nanoparticles for delivery of BMPs, Journal of Controlled Release 142(3) (2010) 312-318.

[13] D. Cunliffe, C. de las Heras Alarcón, V. Peters, J.R. Smith, C. Alexander, Thermoresponsive Surface-Grafted Poly(N−isopropylacrylamide) Copolymers: Effect of Phase Transitions on Protein and Bacterial Attachment, Langmuir 19(7) (2003) 2888–2899.

[14] K. Nagase, J. Kobayashi, A. Kikuchi, Y. Akiyama, H. Kanazawa, T. Okano, Thermally-modulated on/off-adsorption materials for pharmaceutical protein purification, Biomaterials 32(2) (2011) 619-627.

[15] K. Yoshizako, Y. Akiyama, H. Yamanaka, Y. Shinohara, Y. Hasegawa, E. Carredano, A. Kikuchi, T. Okano, Regulation of Protein Binding toward a Ligand on Chromatographic Matrixes by Masking and Forced-Releasing Effects Using Thermoresponsive Polymer, Anal. Chem. 74(16) (2002) 4160–4166.

[16] E. Psarra, U. König, Y. Ueda, C. Bellmann, A. Janke, E. Bittrich, K.-J. Eichhorn, P. Uhlmann, Nanostructured Biointerfaces: Nanoarchitectonics of Thermoresponsive Polymer Brushes Impact Protein Adsorption and Cell Adhesion, ACS Appl. Mater. Interfaces 7(23) (2015) 12516–12529.

[17] A. Papagiannopoulos, A. Meristoudi, K. Hong, S. Pispas, Kinetics of temperature response of PEO-b-PNIPAM-b-PAA triblock terpolymer aggregates and of their complexes with lysozyme, Polymer 83 (2016) 111-115.

[18] A. Papagiannopoulos, A. Meristoudi, S. Pispas, U. Keiderling, Thermoresponsive behavior of micellar aggregates from end-functionalized PnBA-b-PNIPAM-COOH block copolymers and their complexes with lysozyme, Soft Matter 12(31) (2016) 6547-6556.

[19] J. Škvarla, J. Zedník, M. Šlouf, S. Pispas, M. Štěpánek, Poly(N-isopropyl acrylamide)-block-poly(n-butyl acrylate) thermoresponsive amphiphilic copolymers: Synthesis, characterization and self-assembly behavior in aqueous solutions, European Polymer Journal 61 (2014) 124-132.

[20] J. Fitter, T. Gutberlet, J. Katsaras, Neutron Scattering in Biology: Techniques and Applications, Spinger2006.

[21] B.J. Berne, R. Pecora, Dynamic Light Scattering, With Applications to Chemistry, Biology, and Physics, Dover, Toronto, 2000.

[22] U. Keiderling, The new 'BerSANS-PC' software for reduction and treatment of small angle neutron scattering data, Applied Physics A 74(1) s1455-s1457.

[23] J.G. Barker, J.S. Pedersen, Instrumental Smearing Effects in Radially Symmetric Small-Angle Neutron Scattering by Numerical and Analytical Methods, J. Appl. Crystallogr. 28 (1995) 105-114.

[24] D. Vanderbilt, S.G. Louie, A Monte carlo simulated annealing approach to optimization over continuous variables, Journal of Computational Physics 56(2) (1984) 259-271.

[25] C. Wu, S. Zhou, Laser Light Scattering Study of the Phase Transition of Poly(N4sopropylacrylamide) in Water. 1. Single Chain, Macromolecules 28 (1995) 8381-8387.

[26] Q. Zhang, C. Weber, U.S. Schubert, R. Hoogenboom, Thermoresponsive polymers with lower critical solution temperature: from fundamental aspects and measuring techniques to recommended turbidimetry conditions, Materials Horizons 4(2) (2017) 109-116.

[27] J. Zhao, G. Zhang, S. Pispas, Thermoresponsive brush copolymers with poly(propylene oxide-ran-ethylene oxide) side chains via metal-free anionic polymerization "grafting from" technique, Journal of Polymer Science Part A: Polymer Chemistry 48(11) (2010) 2320-2328.

[28] A. Papagiannopoulos, J. Zhao, G. Zhang, S. Pispas, A. Radulescu, Thermoresponsive transition of a PEO-b-PNIPAM copolymer: From hierarchical aggregates to well defined ellipsoidal vesicles, Polymer 54(23) (2013) 6373-6380.

[29] G. Beaucage, Approximations Leading to a Unified Exponential/Power-Law Approach to Small-Angle Scattering, Journal of Applied Crystallography 28(6) (1995) 717-728.

[30] B. Hammouda, Analysis of the Beaucage model, Journal of Applied Crystallography 43(6) (2010) 1474-1478.

[31] A. Papagiannopoulos, J. Zhao, G. Zhang, S. Pispas, A. Radulescu, Thermoresponsive aggregation of PS–PNIPAM–PS triblock copolymer: A combined

study of light scattering and small angle neutron scattering, European Polymer Journal 56 (2014) 59-68.

[32] G. Beaucage, T.A. Ulibarri, E.P. Black, D.W. Schaefer, Multiple Size Scale Structures in Silica—Siloxane Composites Studied by Small-Angle Scattering, Hybrid Organic-Inorganic Composites1995, pp. 97–111.

[33] P. Schmidt, Small-angle scattering studies of disordered, porous and fractal systems, Journal of Applied Crystallography 24(5) (1991) 414-435.

[34] S.K. Filippov, A. Bogomolova, L. Kaberov, N. Velychkivska, L. Starovoytova, Z. Cernochova, S.E. Rogers, W.M. Lau, V.V. Khutoryanskiy, M.T. Cook, Internal Nanoparticle Structure of Temperature-Responsive Self-Assembled PNIPAM-b-PEG-b-PNIPAM Triblock Copolymers in Aqueous Solutions: NMR, SANS, and Light Scattering Studies, Langmuir 32(21) (2016) 5314–5323.

[35] H. JS, B. HC., Polymers and neutron scattering, OUP1994.

[36] P. Lijnzaad, H.J.C. Berendsen, P. Argos, A method for detecting hydrophobic patches on protein surfaces, Proteins: Structure, Function, and Bioinformatics 26(2) (1996) 192-203.